Multiresolution-Based Pansharpening in Spectral Color Images

Oili Kohonen, School of Computing, University of Eastern Finland, Joensuu, Finland

Abstract

This work examines the spectrum preserving properties of a multi-resolution analysis-based intensity modulation (MRAIM) when used for increasing the spatial resolution of spectral color images. The MRAIM algorithm is originally designed to fuse high-resolution panchromatic images with low-resolution spectral images in order to get high-resolution spectral images for remote sensing applications. Instead of panchromatic images, for which the MRAIM algorithm has originally been designed for, the MRAIM algorithm is implemented to use information from both grayscale and RGB color images. In order to utilize the information of the three channels included in RGB images, two different models are derived and examined. In addition, two kind of scaling factors are used for compensating possible differences between the images acquired at different resolution levels. The resulting high resolution spectral images are compared to the real acquired high resolution spectral images with respect to both maximum and average RMS errors and ΔE^*_{ab} *color differences under CIE illuminants* D_{65}*, A, F8 and F11. The used images are acquired by NuanceFX spectral imaging system, which allows the measuring of both spectral and RGB images at different resolution levels at identical geometry.*

Introduction

Image fusion aims at the integration of disparate and complementary data to enhance the information apparent in the images as well as to increase the reliability of the interpretation [1]. In digital imagery, image fusion is applied in order to sharpen images, improve geometric corrections, provide stereo-viewing capabilities, replace defective data, substitute missing information, enhance certain features and complement data sats for improved classification [1]. Detailed reviews on image fusion methods and technology are given by Pohl and van Genderen [1], and Smith and Heather [2].

In the area of remote sensing a large number of image fusion methods have been proposed for combining high-resolution panchromatic images and low-resolution spectral images in order to generate high-resolution spectral images. According to Thomas *et al.* [3], the ideal fusion method should be able to preserve original spectral and spatial information of the multi-spectral images while increasing the spatial resolution. Furthermore, according to Wald *et al.* [4] the resulting fused high-resolution spectral image should be as identical as possible to the real high-resolution spectral image that would be observed by spectral sensors at high resolution level. However, in the case of image fusion processes, there usually is no such ideal reference image into which the fused image could be compared. Thus, quality assessment of used images is often carried out by human visual inspection [5]. Many different image quality measurements such as MI (mutual information) [6], OEFP (objective evaluation of fusion performance) [7], and IFQI (image fusion quality index) [8] have been developed, but the variety of different application requirements and the lack of a clearly defined ground-truth complicate the objective performance assessment [9]. There neither exists an ideal fusion method and thus the fused images are thought as tradeoffs between a good geometrical representation of structures and a good representation of original colors [10]. For an example, methods based on PCA and Brovey transforms [11], provide superior visual high resolution spectral images but ignore the requirement of a high quality synthesis of spectral information [12].

Among the various frameworks in which image fusion has been formulated, the multiresolution approach is one of the most intensively studied and used [13]. A multi-resolution based pan-sharpening has gained a lot of interest lately in the area of remote sensing, since it has given promising results in respect to preserving the spectral information. Furthermore, it also has advantages of being time efficient and rather easy to implement. Within the visual spectral imaging, spectral image fusion as been applied for improving face recognition under constant and varying illumination [14, 15], and improving the texture in endoscope images [16].

This work examines the spectrum preserving properties of a multi-resolution analysis-based intensity modulation [17] which is used for pansharpening in remote sensing applications. The experiments are based on the use of spectral and RGB images of both high and low spatial resolution. The used images are acquired by NuanceFX spectral imaging system [18], which allows the measuring of both spectral and RGB images at different resolution levels at identical geometry. The spatial resolution of low resolution spectral images is increased by MRAIM method using high resolution grayscale images which correspond to panchromatic images and are generated from acquired high resolution RGB images as averages over the three channels. Next, the resolution is increased by using RGB images and the applicability of two different approaches of utilizing RGB images in the MRAIM algorithm is examined. The resulting high resolution spectral images are compared to the real acquired high resolution spectral images with respect to both RMS errors and ΔE^*_{ab} color differences under CIE illuminants D_{65}, A, F8 and F11. In addition, the problematic cases from the algorithm point of view are defined in discussion.

MRAIM fusion

Multiresolution analysis-based intensity modulation (MRAIM) introduced by Wang *et al.* [17] is designed to fuse a high-resolution panchromatic image with a low-resolution spectral image in order to get a high-resolution spectral image. The starting point is the following assumption according to which the proportion of pixels of high and low resolution panchromatic images ($DN_{high}(\lambda_{PAN})$ & $DN_{low}(\lambda_{PAN})$) relates to the proportion of pixels of high and low resolution spectral images ($DN_{high}(\lambda_{MS})$ & $DN_{low}(\lambda_{MS})$).

$$\frac{DN_{high}(\lambda_{PAN})}{DN_{low}(\lambda_{PAN})} = \frac{DN_{high}(\lambda_{MS})}{DN_{low}(\lambda_{MS})} \quad (1)$$

which yields

$$DN_{high}(\lambda_{MS}) = \frac{DN_{high}(\lambda_{PAN})}{DN_{low}(\lambda_{PAN})} DN_{low}(\lambda_{MS}) \quad (2)$$

In order to avoid problems arising in the case of $\mathrm{DN_{low}}(\lambda_{\mathrm{PAN}}) = 0$ Equation 2 is transferred into the following form

$$DN_{high}(\lambda_{MS}) = DN_{low}(\lambda_{MS}) + \alpha w \quad (3)$$

in which w is a difference between high- and low-resolution images,

$$w = DN_{high}(\lambda_{PAN}) - DN_{low}(\lambda_{PAN}) \quad (4)$$

and is sometimes also called as wavelet plane [19]. Furthermore, α is defined as,

$$\alpha = \begin{cases} 1, & \text{if } DN_{low}(\lambda_{PAN}) = 0 \\ \frac{DN_{low}(\lambda_{MS})}{DN_{low}(\lambda_{PAN})}, & \text{if } DN_{low}(\lambda_{PAN}) \neq 0 \end{cases} \quad (5)$$

and is referred as the modulation coefficient for the detailed information.

$\mathrm{DN_{high}}(\lambda_{\mathrm{MS}})$ can be calculated as long as $\mathrm{DN_{low}}(\lambda_{\mathrm{PAN}})$ is approximated. Many different methods can be used for calculation of $\mathrm{DN_{low}}(\lambda_{\mathrm{PAN}})$ from $\mathrm{DN_{high}}(\lambda_{\mathrm{PAN}})$, and a paper focusing on this issue can be found in [12].

High resolution panchromatic image $\mathrm{DN_{high}}(\lambda_{\mathrm{PAN}})$ can be thought as grayscale image, which can be generated from a high resolution RGB image, $\mathrm{DN_{high}}(\lambda_{\mathrm{RGB}})$, as average over the three channels.

$$DN_{high}(\lambda_{PAN}) = \frac{1}{3}\sum_{i=1}^{3} DN_{high}(\lambda_{RGBi}) \quad (6)$$

Using the three channels

The previous equations are based on the use of panchromatic images consisting of one channel. If RGB-images, which consist of three channels, are employed, the above equations must be modified. In these experiments two methods are applied.

Method 1

In the first method a panchromatic image is replaced by one of the RGB channels, depending on the wavelength of the spectral channel to be processed.

$$w(\lambda) = DN_{high}(\lambda_k) - DN_{low}(\lambda_k) \quad (7)$$

and

$$k = \begin{cases} R, & \text{if } \lambda > 600 \text{ nm} \\ B, & \text{if } \lambda < 520 \text{ nm} \\ G, & \text{otherwise} \end{cases} \quad (8)$$

Furthermore, α is defined as follows

$$\alpha(\lambda) = \begin{cases} 1, & \text{if } DN_{low}(\lambda_k) = 0 \\ \frac{DN_{low}(\lambda_{MS})}{DN_{low}(\lambda_k)}, & \text{if } DN_{low}(\lambda_k) \neq 0 \end{cases} \quad (9)$$

and k is defined as above.

Method 2

In the second method panchromatic image is replaced by the weighted combination of the RGB channels. The weights used are dependent on the wavelength of the spectral channel to be processed. Hypothetically, the used weights should be proportional to the sensitivities of the used camera system. However, because of the current unavailability of the camera sensitivities due to some practical equipment related issues, the color matching functions are applied instead.

$$w(\lambda) = \sum_{k=R}^{B} \beta(\lambda_k)(DN_{high}(\lambda_k) - DN_{low}(\lambda_k)) \quad (10)$$

and

$$\beta(\lambda_k) = \begin{cases} \frac{\bar{x}(\lambda)}{\bar{x}(\lambda)+\bar{y}(\lambda)+\bar{z}(\lambda)}, & \text{if k=R} \\ \frac{\bar{y}(\lambda)}{\bar{x}(\lambda)+\bar{y}(\lambda)+\bar{z}(\lambda)}, & \text{if k=G} \\ \frac{\bar{z}(\lambda)}{\bar{x}(\lambda)+\bar{y}(\lambda)+\bar{z}(\lambda)}, & \text{if k=B} \end{cases} \quad (11)$$

in which $\bar{x}(\lambda)$, $\bar{y}(\lambda)$ and $\bar{z}(\lambda)$ are the color matching functions. Using this method, $\alpha(\lambda)$ is defined as

$$\alpha(\lambda) = \begin{cases} 1, & \text{if } DN_{low}(\lambda_k) = 0 \\ \frac{DN_{low}(\lambda_{MS})}{\Sigma_{k=R}^{B} DN_{low}(\lambda_k)}, & \text{if } DN_{low}(\lambda_k) \neq 0 \end{cases} \quad (12)$$

Scaling factors

The scaling factor S is used in order to compensate the differences in spectra acquired at different resolution levels. Applicability of two different scaling factors is examined and these scaling factors S_1 and S_2 are defined as follows.

$$S_1 = (DN_{high}(\lambda_{PAN}) - DN_{low}(\lambda_{PAN}))./255 \quad (13)$$

$$S_2 = \frac{DN_{high}(\lambda_{PAN})}{DN_{low}(\lambda_{PAN})} \quad (14)$$

In the case of S_1 Equation 3 can be written as

$$DN_{high}(\lambda_{MS}) = (S_1 + 1)DN_{low}(\lambda_{MS}) + \alpha w \quad (15)$$

and in the case of S_2 Equation 3 is defined as

$$DN_{high}(\lambda_{MS}) = S_2 DN_{low}(\lambda_{MS}) + \alpha w \quad (16)$$

Experiments

Acquired images

In these experiments two objects were acquired by Nuance FX multispectral imaging system [18], which allows the measuring of both spectral and RGB color images at three resolution levels. The images were acquired with a geometry 45/0, 45 and 0 being the angles between the normal of the measured surface and the incident light, and the normal of the measured surface and the capturing device, respectively. Both spectral and RGB color images were taken at two resolution levels and the the sizes of the produced images were 520x696 and 1040x1392 pixels. The objects were measured under D_{65} light source of Gretag Macbeth SpectraLight III light booth, and in the case of spectral images the used wavelength range was from 420nm to 720nm at 10nm intervals. The acquired objects were cardboard image of lasagna portion and part of Gretag Macbeth ColorChecker. The objects are shown in an RGB format in Fig. 1 and are from now referred as "chart" and "food". Due to the low spectral radiance of the used light source at the beginning of the blue region of the spectrum and due to the possible lower sensitivity of the used camera system at the very same region, the first two channels contained

too much noise and thus, were not used in experiments. In order to distinguish the color differences between the real high resolution spectral image and the estimated high resolution spectral image into the differences originated from the discrepancy between acquired spectra at low and high resolution levels and the differences resulted while increasing the spatial resolution, the RMS errors and ΔE^*_{ab} color differences between the acquired high and low resolution spectral images were calculated. The maximum and average ΔE^*_{ab} color differences under D_{65}, A, F8 and F11 are shown in Table 1. In addition, the maximum and average RMS errors are 0.0841 & 0.0085 in the case of "chart", and 0.0742 & 0.0093 in the case of "food".

Color differences								
	under A		under D_{65}		F8		F11	
Image	max	ave	max	ave	max	ave	max	ave
chart	16.3	1.6	16.0	1.5	16.4	1.5	19.3	1.8
food	11.9	1.9	12.1	1.8	11.3	1.8	12.7	2.1

Table 1. Maximum and average ΔE^*_{ab} color differences between the spectral images acquired at high and medium resolution levels.

Enhancing using grayscale images

In the first part of the experiments the spatial resolution of low resolution spectral images was enhanced by using high resolution grayscale images. The enhancing process was performed according to the original pansharpening approach used widely for remote sensing images. Since the real acquired panchromatic images were not available, the grayscale images, created from the acquired RGB images as averages over the three color channels, were used.

The low resolution images needed in Equation 3 were generated from the high resolution image as averages of 2×2 pixel areas. In addition, acquired low resolution RGB images transformed into the grayscale form were also used. These two kind of low resolution images used are referred in the below Tables as "calculated" and "measured" low resolution images. Furthermore, the spatial resolution was enhanced both with and without scaling. The maximum and average ΔE^*_{ab} color differences between the acquired and estimated high resolution spectral images are shown in Table 2, and maximum and average RMS errors can be found as a part of Tables 4 ("chart") and 6 (food"). In each of these Tables, the used scaling methods are referred as S_0-S_2. In the cases of S_1 and S_2 scalings presented in Equations 15 and 16 are performed, whereas in the case of S_0 no scaling is used. ΔE^*_{ab} color differences between acquired and estimated high resolution "chart" images in the case of enhancing based on grayscale image are shown in a pictorial form in the first part of Fig. 2. Furthermore, an example of acquired and estimated spectra are shown in Fig. 3.

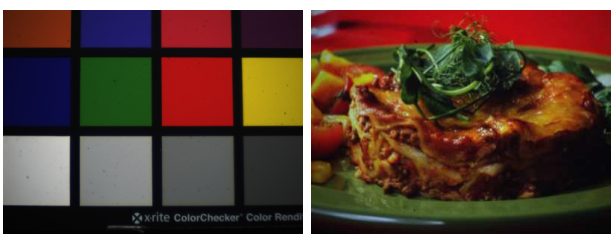

Figure 1. *Acquired images ("chart" and "food") in an RGB format.*

Color differences (chart)								
Calculated low resolution image								
chart	under D_{65}		under A		under F8		under F11	
method	max	ave	max	ave	max	ave	max	ave
S_0	22.6	1.6	21.9	1.6	22.0	1.6	25.2	1.9
S_1	21.9	1.6	21.0	1.6	21.0	1.6	24.0	1.9
S_2	19.8	1.7	19.1	1.6	17.7	1.6	19.5	1.9
Measured low resolution image								
chart	under D_{65}		under A		under F8		under F11	
method	max	ave	max	ave	max	ave	max	ave
S_0	22.6	1.6	21.9	1.6	22.0	1.6	25.1	1.9
S_1	21.8	1.6	21.0	1.6	21.0	1.6	24.0	1.9
S_2	19.5	1.7	18.9	1.6	17.6	1.6	19.3	1.9
Color differences (food)								
Calculated low resolution image								
food	under D_{65}		under A		under F8		under F11	
method	max	ave	max	ave	max	ave	max	ave
S_0	12.0	1.8	12.3	1.7	12.0	1.7	15.2	2.0
S_1	11.6	1.7	11.9	1.6	11.6	1.6	14.4	1.9
S_2	10.8	1.7	11.3	1.7	10.5	1.7	11.2	1.9
Measured low resolution image								
food	under D_{65}		under A		under F8		under F11	
method	max	ave	max	ave	max	ave	max	ave
S_0	13.2	1.8	13.1	1.7	12.8	1.7	16.1	2.0
S_1	12.7	1.7	13.0	1.6	12.4	1.6	15.3	1,9
S_2	10.9	1.7	11.6	1.7	10.5	1.7	12.0	1.9

Table 2. Maximum and average ΔE^*_{ab} color differences between the estimated and acquired high resolution spectral images under CIE illuminants D_{65}, A, F8 and F11. The enhancing has been done using grayscale images.

Enhancing using RGB images

In the second part of the experiments the spatial resolution of low resolution spectral images was enhanced by using high resolution RGB images. Based on the assumption, the use of information from three channels instead of one would improve the accuracy of estimated spectra. As described in the previous section, two different methods were used in order to utilize the information from three channels, and from now on these methods are referred as M1 and M2. In M1, the panchromatic images of the MRAIM model were replaced by one of the RGB channels, depending on the wavelength of the spectral channel to be processed. In M2, the panchromatic images were replaced by the weighted combination of the RGB channels, as explained in Equations 10 -12. The calculations were performed both with and without scaling. For RGB images the scaling factors were calculated as averages of scaling factors of each channel. The maximum and average ΔE^*_{ab} color differences between the acquired and estimated high resolution spectral images are shown in Tables 3 and 5, and maximum and average RMS errors can be found as a part of Tables 4 ("chart") and 6 (food"). ΔE^*_{ab} color differences between acquired and estimated high resolution "chart" images in the case of enhancing based on RGB image and methods M1 & M2 are shown in a pictorial form in Fig. 2. Furthermore, an example of acquired and estimated spectra are shown in Fig. 3.

Discussion & Conclusions

The spectrum preserving properties of a multi-resolution analysis-based intensity modulation (MRAIM) when used for increasing the spatial resolution of spectral images. was examined in this work. In the performed experiments, two spectral images of low spatial resolution were transformed into

Color differences (chart, M1)								
Calculated low resolution image								
chart	under D_{65}		under A		under F8		under F11	
method	max	ave	max	ave	max	ave	max	ave
S_0	11.7	1.8	10.6	1.7	11.7	1.7	13.9	2.0
S_1	12.2	1.8	11.1	1.7	12.0	1.8	14.1	2.0
S_2	31.2	1.9	32.3	1.9	32.6	1.9	36.2	2.2
Measured low resolution image								
food	under D_{65}		under A		under F8		under F11	
method	max	ave	max	ave	max	ave	max	ave
S_0	14.2	2.3	12.7	2.3	13.5	2.3	16.5	2.5
S_1	14.2	2.4	13.0	2.3	13.8	2.3	16.5	2.5
S_2	30.7	2.5	31.9	2.4	32.4	2.5	35.5	2.7
Color differences (chart, M2)								
Calculated low resolution image								
food	under D_{65}		under A		under F8		under F11	
method	max	ave	max	ave	max	ave	max	ave
S_0	10.3	1.6	9.5	1.5	10.3	1.5	13.3	1.8
S_1	10.4	1.6	9.8	1.5	10.3	1.6	13.2	1.8
S_2	27.0	1.7	29.0	1.7	29.3	1.7	33.2	2.0
Measured low resolution image								
food	under D_{65}		under A		under F8		under F11	
method	max	ave	max	ave	max	ave	max	ave
S_0	11.2	1.8	10.7	1.8	11.1	1.8	14.0	2.0
S_1	11.4	1.8	11.0	1.8	11.2	1.8	14.0	2.1
S_2	26.7	2.0	28.9	2.0	29.2	2.0	32.7	2.3

Table 3. Maximum and average ΔE^*_{ab} color differences between the estimated and acquired high resolution spectral images under CIE illuminants D_{65}, A, F8 and F11. The enhancing has been done using RGB images.

RMS errors (chart)						
Calculated low resolution image						
chart	grayscale		RGB M1		RGB M2	
method	max	ave	max	ave	max	ave
S_0	0.0910	0.0072	0.0409	0.0082	0.0413	0.0080
S_1	0.0777	0.0073	0.0507	0.0087	0.0496	0.0086
S_2	0.0551	0.0076	0.0945	0.0099	0.0938	0.0097
Measured low resolution image						
chart	grayscale		RGB M1		RGB M2	
method	max	ave	max	ave	max	ave
S_0	0.0910	0.0072	0.0461	0.0097	0.0448	0.0092
S_1	0.0778	0.0074	0.0607	0.0103	0.0589	0.0099
S_2	0.0551	0.0077	0.1016	0.0117	0.0999	0.0112

Table 4. Maximum and average RMS errors between the estimated and acquired high resolution spectral images.

Color differences (food, M1)								
Calculated low resolution image								
chart	under D_{65}		under A		under F8		under F11	
method	max	ave	max	ave	max	ave	max	ave
S_0	9.8	1.8	10.1	1.7	9.8	1.8	12.5	2.0
S_1	9.6	1.8	9.5	1.7	9.5	1.7	12.4	1.9
S_2	11.6	1.9	11.2	1.8	11.3	1.9	12.9	2.1
Measured low resolution image								
chart	under D_{65}		under A		under F8		under F11	
method	max	ave	max	ave	max	ave	max	ave
S_0	11.9	2.1	10.4	1.9	11.5	1.9	11.7	2.1
S_1	11.9	2.1	10.4	1.9	11.5	2.0	11.7	2.2
S_2	13.6	2.3	12.8	2.2	12.8	2.2	14.0	2.4
Color differences (food, M2)								
Calculated low resolution image								
food	under D_{65}		under A		under F8		under F11	
method	max	ave	max	ave	max	ave	max	ave
S_0	8.6	1.6	8.4	1.6	8.7	1.6	12.0	1.8
S_1	9.0	1.6	8.6	1.5	9.0	1.5	12.0	1.8
S_2	12.0	1.8	11.4	1.7	12.3	1.7	13.8	2.0
Measured low resolution image								
food	under D_{65}		under A		under F8		under F11	
method	max	ave	max	ave	max	ave	max	ave
S_0	7.8	1.5	8.3	1.5	7.8	1.5	9.6	1.7
S_1	7.8	1.6	8.3	1.5	7.8	1.5	9.6	1.7
S_2	12.2	1.9	11.6	1.8	12.2	1.8	13.9	2.1

Table 5. Maximum and average ΔE^*_{ab} color differences between the estimated and acquired high resolution spectral images under CIE illuminants D_{65}, A, F8 and F11. The enhancing has been done using RGB images.

RMS errors (food)						
Calculated low resolution image						
food	grayscale		RGB M1		RGB M2	
method	max	ave	max	ave	max	ave
S_0	0.0807	0.0079	0.0347	0.0082	0.0341	0.0080
S_1	0.0522	0.0071	0.0673	0.0080	0.0699	0.0078
S_2	0.0855	0.0083	0.1277	0.0105	0.1299	0.0105
Measured low resolution image						
food	grayscale		RGB M1		RGB M2	
method	max	ave	max	ave	max	ave
S_0	0.0807	0.0079	0.045	0.0073	0.0317	0.0067
S_1	0.0523	0.0072	0.0728	0.0078	0.0742	0.0073
S_2	0.0855	0.0084	0.1362	0.0114	0.1385	0.0111

Table 6. Maximum and average RMS errors between the estimated and acquired high resolution spectral images.

spectral images of high spatial resolution by using MRAIM algorithm, which is used in remote sensing applications for increasing the spatial resolution of spectral images. In the performed experiments both high resolution grayscale and RGB images were employed.

In the case of grayscale images, the use of acquired low resolution image instead of calculated low resolution image seems not to make any real difference. When considering the maximum color difference, the use of scaling clearly seems to lower the differences. However, the same does not hold true in the case of average color differences, according to which no clear benefit is achieved by using either of the scaling methods. The similar observations can be done also in the case of RMS errors. The use of scaling lowers considerably the maximum errors, but also cause some increase in the average RMS values.

In the case of RGB images, the use of S_2 scaling increases notably both maximum and average color differences and RMS errors between the acquired and estimated high resolution spectral images. In addition, neither the other scaling method seems to give any clear benefit. When comparing methods M1 and M2 to each other, the results achieved are congruent in the case of RMS errors. However, in the case of color differences, the lower differences are achieved by using method M2.

The main point, however, is what in general happens when the spatial resolution of low resolution spectral images is enhanced. At the beginning, the average color differences between the low resolution spectral image and the high resolution spectral image, whose resolution was lowered to the size of the low resolution spectral image, were in the case of "chart" around 1.5-1.6 for D_{65}, A and F8, and 1.8 for F11, which generally produces higher errors). In the case of "food", these values were 1.8-1.9 for D_{65},

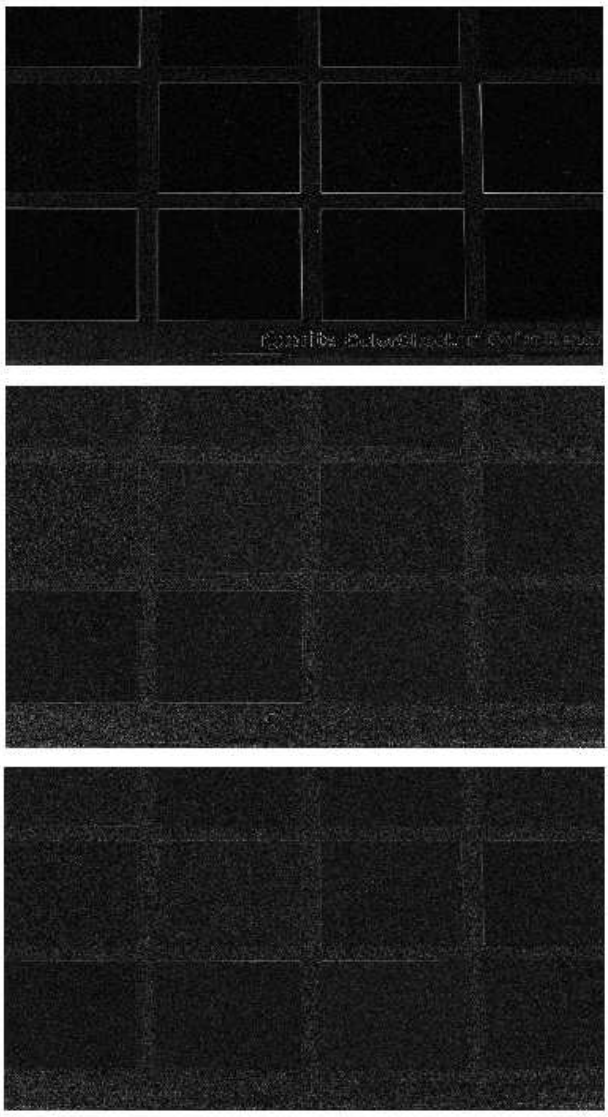

Figure 2. *The resulted color differences between the enhanced and acquired high resolution spectral images in a pictorial form. Enhancing has been done by using a) grayscale image , b) RGB image and method M1 and c) RGB image and method M2. The images have been scaled to use the whole gray colormap.*

A and F8, and 2.1 for F11. In the case of enhancing by grayscale images without any scalings the corresponding numbers are 1.6 and 1.7-1.8 for D_{65}, A and F8, and 1.9 and 2.0 for F11 in the cases of ”chart” and ”food”, respectively. For enhancing using RGB image and method M1, the numbers are 1.7-1.8 for D_{65}, A and F8, and 2.0 for F11 for both ”chart” and ”food” images. Furthermore, for RGB images and method M2, the numbers are even a bit lower - in the case of ”chart” 1.5-1.6 for D_{65}, A and F8, and 1.8 for F11, whereas in the case of ”food” 1.6 for D_{65}, A and F8, and 1.8 for F11. Thus, based on the color differences, the enhancing process without scalings seems to work quite nicely. Furthermore, when comparing the enhanced images to the acquired high resolution images, the RMS errors are smaller than the ones achieved by comparing the original, acquired images which are transferred into the low resolution level.

From a Fig. 2, in which the achieved color differences are

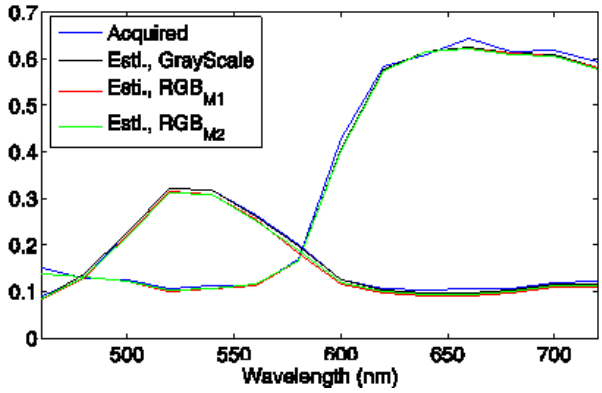

Figure 3. *An example of two spectra of a high resolution spectral image and spectra estimated by MRAIM algorithm using grayscale image, RGB image and method M1 and RGB image and method M2.*

presented in a pictorial form for image ”chart”, one can notice that the largest color differences, are on those areas in which one color is changing into another color. This is caused by the fact that the grayscale images which are taken as averages over the channels of acquired RGB images are not able to provide enough information about the changes in color content. As an example, let us assume RGB triplet of values [200 100 0]. In grayscale image this triplet would be presented as (200+100+0)/3=100. Furthermore, let us assume that in the next RGB triplet the values are [220 80 0]. The grayscale presentation equals to the previous one even though the two triplets are not the same. As a result, the wavelet plane w which is used in MRAIM algorithm to provide the information about the difference between high- and low-resolution images, is not always really able to extract the required information.

One can distinguish between two problematic cases. In the first one, the compared gray level pixels in the high and low resolution images are identical but the corresponding RGB triplets are not alike, as described above. In this case, the wavelet plain w equals to zero and thus, the high resolution pixel to be estimated (according to Equation 3) equals to the previous low resolution pixel. In the other case, the changes in RGB triplets are transferred to the grayscale presentation and the wavelet plain no longer equals to zero. However, the information transferred to the modulation coefficient α, includes only the information about lightness changes and thus each wavelength of the spectra of low resolution image is put through the same changes (according to Equation 3). The issue is problematic but is emphasized only on the border areas of the colors. In the examined models M1 and M2, the use of three different channels allows the handling of color information at different parts of spectra. This removes the problems classified to case one above and reduces the problems classified to the previously mentioned case two. From Fig. 2 one can notice that in the cases where RGB images have been used the clear straight lines of color difference does not exist anymore. This is good, but there is also a shortcoming. As stated before, when RGB images are used instead of grayscale image the average color difference is a bit higher even though a tremendous lowering is achieved in the cases of maximum color differences. The three images presented in Fig. 2 are scaled to use the whole gray color map. Thus, these images are not comparable as such, but each image shows the distribution of color differences in that certain image.

MRAIM method is time efficient and rather easy to implement. It obviously has some shortcomings as described above, but based on the performed experiments, it preserves the spectral properties pretty well. Of course, this study was based on only two images, which were chosen to be rather simplified objects. The work needed to be done in the future would be the examination of more challenging objects, in which the details and the areas of solid colors are very tiny. Furthermore, the use of camera sensitivities instead of color matching functions would be recommended.

Acknowledgements

The funding from Kordelin Foundation is gratefully appreciated.

References

[1] C. Pohl, and J. L. van Genderen, Multisensor Image Fusion in Remote Sensing: Concepts, Methods and applications, Int. J. Remote Sensing, 19, 823 (1998).

[2] M. I. Smith, and J. P. Heather, Review of Image Fusion Technology in 2005, Proc. SPIE, pg. 29. (2005)

[3] C. Thomas, T. Ranchin, L. Wald, and J. Chanussot, Synthesis of Multispectral Images to High Spatial Resolution: a Critical Review of Fusion Methods Based on Remote Sensing Physics, Trans. Geosci. Rem. Sens., 46, 2008.

[4] J. Wald, T. Ranchin, and M. Mangolini, Fusion of Satellite Images of Different Spatial Resolutions: Assessing the Quality of Resulting Images, Photogramm. Eng. Remote Sens., 46, 1325 (1997).

[5] A. Toet, and E. M. Franken, Perceptual Evaluation of Different Image Fusion Schemes, Displays, 24, 25 (2003).

[6] G. Qu, D. Zhang, and P. Yan, Information Measure for Performance of Image Fusion, Electron. Lett., 38, 313 (2002).

[7] V. S. Petrovic, and C. S. Xydeas, Sensor Noise Effects on Signal-Level Image Fusion Performance, Inf. Fusion, 4, 167 (2003).

[8] G. Piella, New Quality Measures for Image Fusion, Proc. of the 7th International Conference on Information Fusion, pg. 542. (2004).

[9] G. Piella, and H. Heijmans, A New Quality Metric for Image Fusion, Proc. of International Conference on Image Processing, pg. III-173-6. (2003).

[10] A. Loza, T. D. Dixon, E. F. Canga, S. G. Nikolov, D. R. Bull, C. N. Canagarajah, J. M. Noyes, and T. Troscianko, Methods of Fused Image Analysis and Assessment, Advances and Challenges in Multisensor Data and Information Processing, NATO Security through Science Series, IOS Press, 2007.

[11] P. S. Chavez, S. C. Sides, and J. A. Anderson, Comparison of Three Different Methods to Merge Multiresolution and Multispectral Data: Landsat TM and SPOT Panchromatic, Photogram. Engin. Remote Sensing, 57, 295 (1991).

[12] Z. Wang, D. Ziou, C. Armenakis, D. Li and Q. Li, A Comparative Analysis of Image Fusion Methods, IEEE Trans Geosci Rem Sens, 43, 1391 (2005).

[13] G. Piella Fenoy, Adaptive Wavelets and Their Applications to Image Fusion and Compression, Ponsen & Looijen bv., 2003.

[14] H. Chang, A. Koschan, B. Abidi, and M. Abidi, Physics-Based Fusion of Multispectral Data for Improved Face Recognition, Proc. of 18th International Conference on Pattern Recognition, pg. 1083. (2006).

[15] R. Singha, M. Vatsaa, and A. Noore, Hierarchical Fusion of Multi-Spectral Face Images for Improved Recognition Performance, Information Fusion, 9, 200 (2008).

[16] V. Bochko, Y. Miyake, N. Tsumura, T. Nakaguchi, and J. Parkkinen, Image Fusion in Spectral Electronic Endoscope, Proc. of the 9th International Symposium on Multispectral Colour Science and Application, pg. 109. (2007).

[17] Z. Wang, D. Li, Q. Li, and V. Tao, M-band Wavelet Transform for the Generation of High-Resolution Multispectral Images, Can. J. of Remote Sensing, 34, 33, (2008).

[18] http://www.cri-inc.com/downloads/Nuance_Brochure.pdf

[19] Wang Z., Wavelet Transform Based Multi-Sensor Remote Sensing Image Fusion, PhD thesis, Wuhan University, Wuhan, China, 2002.

Author Biography

Oili Kohonen was born in 1978, in Lappeenranta, Finland. She receiver her M.Sc. and Ph.D. degrees in physics in 2002 and 2007 from the University of Joensuu, Finland.

